Full Length Article

Monte Carlo intercomparison and benchmark of the neutron streaming in the ramified access maze of the CERN High-energy AcceleRator Mixed field (CHARM) facility at CERN

D. Bozzato [a],*, A. Devienne [b], R. Froeschl [a], A. Infantino [a], T. Lorenzon [a], F. Pozzi [a], M. Tisi [a], N. Nakao [c], T. Kajimoto [d], T. Sanami [e], S. Roesler [a], M. Brugger [a]

[a] European Organization for Nuclear Research (CERN), Geneva, Switzerland
[b] Fusion for Energy (F4E), Barcelona, Spain
[c] Institute of Technology, Shimizu Corporation, Tokyo, Japan
[d] Hiroshima University, Hiroshima, Japan
[e] High Energy Accelerator Research Organization (KEK), Ibaraki, Japan

ARTICLE INFO

ABSTRACT

Experiments of high-energy neutron streaming were performed in the access maze of the CERN High-energy AcceleRator Mixed-field (CHARM) facility where high-intensity proton beams of 24 GeV/c impact on a copper target. The streaming of the secondary neutrons through the various legs of the ramified access maze of the facility was measured using aluminium activation detectors installed at 12 different locations: for the first time, the extended coverage of measurement locations allowed to assess the streaming in more distant areas of the maze. The attenuation profile along the maze measured via the production of ^{24}Na was also used to benchmark results from Monte Carlo calculations performed with FLUKA, PHITS, and GEANT4: over almost the five orders of magnitude of the measured production yield, an agreement within a factor 1.4, 1.7, and 2.5 respectively was found for the three codes.

1. Introduction

In recent years, particle accelerator facilities have been constructed for various purposes, notably encompassing fundamental physics research, medical applications, and industrial research and development. To ensure their safe and reliable operation, particularly in the case of high-energy facilities, stringent shielding measures are necessary to minimize stray radiation outside the facilities to levels as low as reasonably achievable. Additionally, all accelerator shields require openings for cables, ventilation ducts, and personnel access. Therefore, the shielding design is a crucial aspect and often a challenging task due to the different constraints that must be taken into consideration. Since the shielding construction costs are often a non-negligible portion of the total cost of a facility, and large modifications are often difficult to implement once the shielding is in place, very reliable tools must be used in the design process.

The design of accelerator facilities in the past days was typically based on semi-empirical formulas (see for instance A. H. Sullivan (1992) [1]). While these approaches can still be useful to provide quick, order-of-magnitude estimates, shielding designs based on these methods tend to be very conservative, leading for instance to higher costs and higher space needs. Nowadays, radiation transport Monte Carlo codes are the state-of-the-art tools utilized in the design and radiation protection assessments of accelerator facilities.

To validate the results obtained from radiation transport codes and to determine more accurately safety margins to be adopted in design studies, benchmarks with experimental data and code intercomparisons are both crucial. At the CERN High-energy AcceleRator Mixed-field (CHARM) facility [2], several experiments covering the deep penetration of neutrons in bulk shielding were conducted with active [3] and passive detectors [4]. In efforts to enhance the availability of experimental data on the streaming of high-energy neutrons (*i.e.*, above 20 MeV) in access mazes of high-energy accelerator facilities, initial measurements were conducted in 2018 [5]: the simulations were found to align with experimental data within a factor of 1.7, and it was additionally observed that, apart from neutron streaming, penetration through the maze walls could significantly contribute to locations further within the maze itself. Owing to the facility configuration and measurement locations at the time, this effect could not be more

precisely quantified. This work presents the series of measurements conducted at CHARM in 2022 which, thanks to the different facility configuration used and the extended coverage of measurement locations, allowed to better assess the neutron streaming in more distant areas of the access maze. In addition, Monte Carlo simulations were performed using three distinct codes, and their outcomes were validated against the experimental data.

2. Experiment

2.1. Facility configuration

The layout of the CHARM facility at the CERN East Experimental Area is depicted in Fig. 1. A 24 GeV/c proton beam, extracted from the CERN Proton Synchrotron (PS), is transported via the T08 beam line through the proton irradiation facility (IRRAD) [6] and then directed to CHARM, where it impacts the centre of the base of a cylindrical target measuring 50 cm in length and 8 cm in diameter. Three different targets are available and are mounted on a remotely controlled revolver: copper, aluminium, and the so-called aluminium sieve which comprises several slits arranged to achieve an effective density approximately one-third that of aluminium. Both the beam line and the centre of the target are positioned at a height of 129 cm above the floor of the experimental area. The target revolver is positioned on a movable table so that, when access is required in the target room, the table can be retracted into a dedicated alcove which is then closed by a 20 cm marble wall: during operation, the marble door remains open. Primary protons that have not interacted with the target are intercepted by a beam dump placed downstream.

Adjacent to the target there are four movable shielding walls, each 20 cm thick. The outer layers are constructed from concrete, while the inner layers consist of cast iron. These walls stand 214 cm high and are utilized to alter the relative particle composition and intensity of the secondary radiation field within the target room during irradiation experiments, or to shield personnel from residual radiation when access to the facility is necessary. Surrounding the beam line and target room is a bulk shielding composed of concrete and cast iron blocks. Access to the target room is only possible through a maze with several legs.

For the experiments described here, the proton beam was always directed at the copper target, which, compared to the other available target choices, produces the most intense secondary field. Additionally, the movable shielding walls were always kept retracted from the target room, thus providing better conditions for the measurements of the neutron streaming even at points further along the maze legs. Indeed, the low energy neutrons downstream of the maze are essentially produced by the scattering of the high-energy ones upstream: removing the shielding walls from the target room allows the high-energy component emitted approximately at 90° from the target to reach the maze without being attenuated by approximately a factor 15. The composition and densities of the shielding materials are detailed in Table 1.

2.2. Experimental set-up

The streaming of neutrons through the various legs of the CHARM access maze was measured via the production of ^{24}Na in activation detectors made of high-purity aluminium (99.999%, 2.7 g/cm^3 density), a material widely used for high-energy neutron measurements. Figs. 2, 3, and 4 illustrate the maze structure and facility configuration during the experiment and provide the detailed location of the installed activation detectors labelled from 0 to 11. Nine activation detectors were mounted at beam height onto custom-made polymethyl methacrylate (PMMA) supports, which were then installed at the horizontal centre of the corridors of the five legs of the maze. Additionally, two detectors, also mounted at beam height on PMMA supports, were positioned at more shielded points in the access maze (locations 0 and 6 as shown in Fig. 4). Finally, one detector was placed in the target room, positioned

Table 1
Density and chemical composition (mass fraction) of the shielding materials used in the present experiment.

Material	Density [g/cm^3]	Element	Mass fraction [%]	Element	Mass fraction [%]
Cast iron	7.3	Fe	92.3	P	0.08
		C	3.85	Co	0.05
		Si	3.4	S	0.02
		Mn	0.3		
Concrete	2.35	O	48.204	Fe	1.263
		Ca	23.929	K	0.833
		Si	16.175	H	0.561
		C	4.377	Na	0.446
		Al	2.113	S	0.414
		Mg	1.512	Ti	0.173

at 90° with respect to the target (location 1 as in Fig. 4). This detector was enclosed in a small plastic bag and hung at approximately 5 cm above the beam height on a hook of the fence delimiting the movable shielding walls: the location defined by the position of this hook is one of the reference irradiation locations of CHARM. Depending on the expected neutron fluence at the corresponding location, two sizes of detectors were used: 4 cm diameter and 0.4 cm thickness samples, and 8 cm diameter and 1 cm thickness samples were employed for locations from 0 to 4 and locations 5 to 11 respectively. Photos of the samples as mounted and installed in the access maze are shown in Fig. 5.

2.3. Beam conditions

The maximum intensity of the proton beam per extraction, or spill, at the time of the experiment was 50×10^{10} protons/spill. The beam intensity is measured using a secondary emission chamber (SEC) located upstream IRRAD and calibrated using the activation foil technique [7]. The SEC counts/spill were retrieved from the CERN Accelerator Logging Service and were then converted to protons/spill using the device calibration factor of 5.46×10^6 protons/count [7,8].

To facilitate the analysis, the data were binned into one-minute intervals to calculate an average beam intensity in protons/s over these fixed-length time windows. The average beam intensity is shown in Fig. 6: the beam irradiation was carried out for about 2 days and 13 h, from the evening of August 26 2022, to the morning of August 29, 2022.

2.4. Gamma spectroscopy and data analysis

After irradiation, the activation detectors were removed from their installation location and transported to the CERN Radio-Analytical Laboratory. Gamma spectroscopy was performed using a high-purity germanium-semiconductor (HPGe) detector, in particular to measure the energy spectrum of photons emitted in the decay of ^{24}Na ($T_{1/2}$ = 14.96 h) produced via the ^{27}Al$(n, \alpha)^{24}$Na reaction in the irradiated samples: the analysed photon energies were 1368.8 keV and 2754.6 keV whose corresponding emission ratios are 1.000 and 0.999. The counting times ranged from 3 to 24 h depending on the peak count rates of the photons from ^{24}Na: the net counts of the photo-peaks at the corresponding photon energies were analysed so that the ^{24}Na production yield could be estimated taking into account the photo-peak efficiencies of the HPGe-detector and the beam intensity during the irradiation as shown in Fig. 6. The analysis methodology adopted was described in detail by Nakao et al. [4], and the efficiencies of the HPGe-detector were estimated in LabSOCS software (Mirion Technologies Canberra KK) [9].
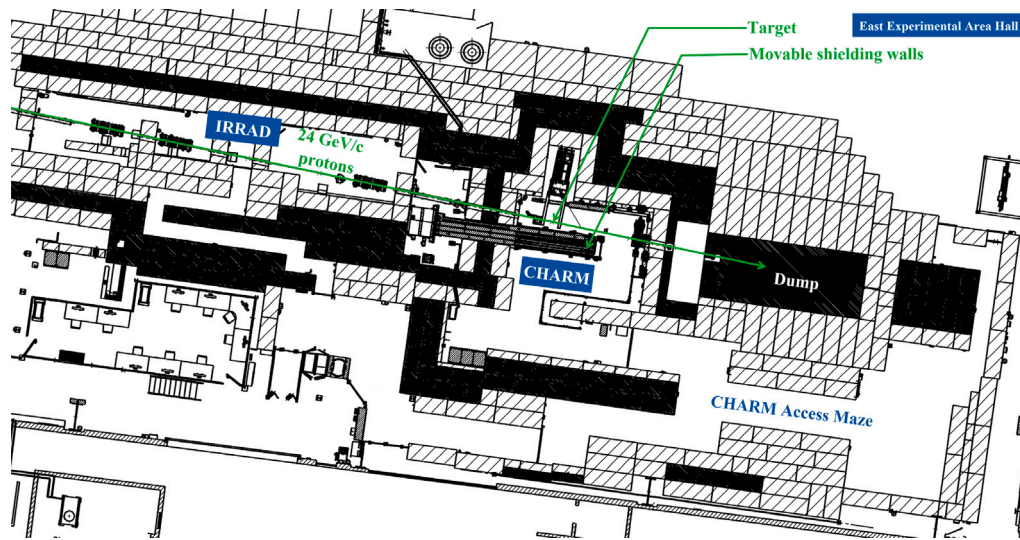
Fig. 1. Engineering drawing of the IRRAD and CHARM facilities at the CERN East Experimental Area: iron and concrete blocks are indicated respectively with a black shading and a diagonal hatching.
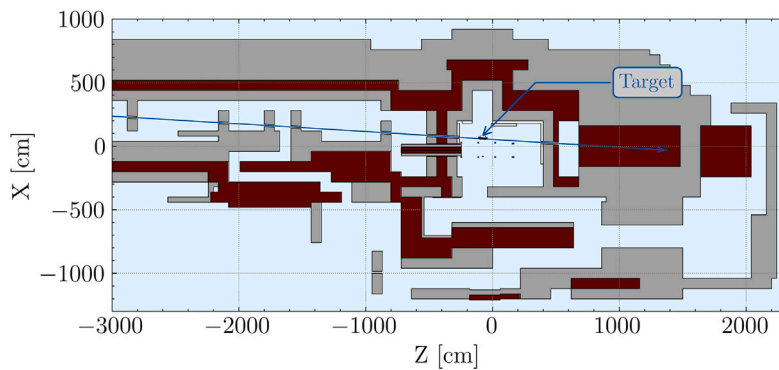

Fig. 2. Horizontal cut at beam level of the simulation geometry. Iron and concrete shielding blocks are depicted respectively in brick-red and grey, while marble walls in white. Arrows indicate the beam direction and the position of the target.
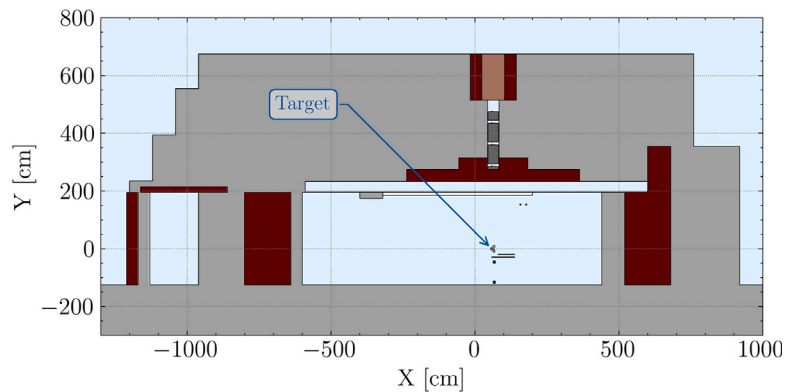

Fig. 3. Vertical cut of the simulation geometry in correspondence of the target. Iron and concrete shielding blocks are depicted respectively in brick-red and grey, while marble walls in white. The arrow indicates the position of the target. The roof shielding, which incorporates the CERN Shielding Benchmark Facility (CSBF) 90° above the target, is also visible: although of minor impact for the experiment described here, the configuration of CSBF consisted of 200 cm concrete (custom-shaped block in darker grey) and 160 cm barite concrete. For a general description of CSBF see for instance N. Nakao et al. [4].
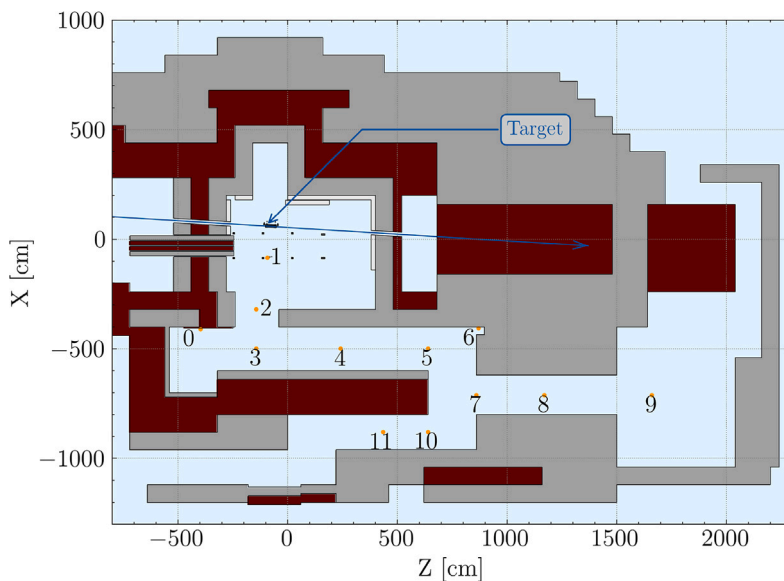
Fig. 4. Horizontal cut at beam level of the simulation geometry with the details of the CHARM facility configuration during the experiments and the installation locations of the activation detectors in the access maze. Iron and concrete shielding blocks are depicted respectively in brick-red and grey, while marble walls in white. Arrows indicate the beam direction and the position of the target.

Fig. 5. Photos of the activation detectors: detectors mounted on the PMMA supports before the installation (left), view of the detector 10, 7, and 8 in the access maze (right).
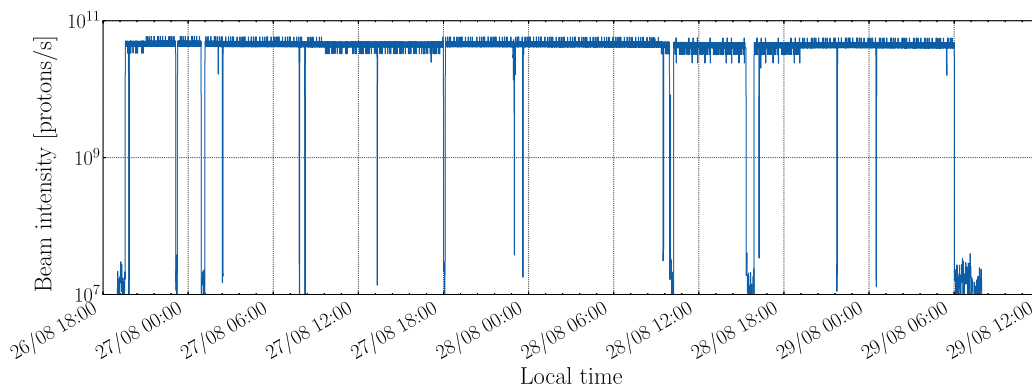

Fig. 6. Average beam intensity sent to the CHARM target during the experiments as monitored with a secondary emission chamber. The intensity is binned in one-minute-long intervals.
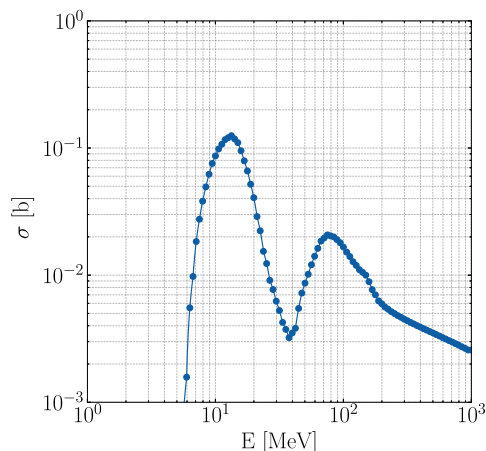
Fig. 7. Cross section of the ^{27}Al$(n,\alpha)^{24}$Na reaction used for the estimation of the ^{24}Na production yield: the cross section is derived from the Maekawa library [24] which is evaluated with data by Kim et al. [25].

Fig. 8. Attenuation profile of the ^{24}Na production yield per ^{27}Al atom and per primary proton [^{24}Na/^{27}Al/proton] as experimentally measured and its comparison with Monte Carlo calculations (MC/Data ratios).

3. Monte Carlo simulation

To benchmark experimental data, Monte Carlo simulations were conducted using the FLUKA code [10,11] (version 4–3.3 distributed by the FLUKA.CERN collaboration), the PHITS code [12,13] (version 3.30), and GEANT4 [14,15] (version 4.11.1).

A detailed description of the physics models implemented in FLUKA can be found in Ref. [10,11]: for neutrons below 20 MeV, the point-wise treatment of neutron transport was enabled using the JEFF-3.3 data library as originally pre-processed for the GEANT4 code [16–19]. For the PHITS simulations, the evaporation model GEM [20], the intra-nuclear cascade model INCL [21] up to 3 GeV, and the high-energy nuclear reaction model JAM [22] above 3 GeV were used, while the JENDL-4.0 data library was used for neutrons below 20 MeV [23]. Finally, the physics list FTFP_BERT_HP was used for the GEANT4 simulations.

The simulations with the three codes were performed with the full geometry of the facility which, in addition to the target room and access maze, includes the upstream IRRAD facility, the 3.6 m thick roof shielding, the 2 m thick concrete floor, and the downstream dump. The FLUKA full simulation geometry's horizontal cut at beam height is depicted in Fig. 2, while the vertical cut including the roof shielding structure is shown in Fig. 3.

The primary source consisted of a 24 GeV/c proton beam with a Gaussian profile having a FWHM of 1.2 cm in the plane perpendicular to the beam direction: this profile was representative of the conditions measured during the experiment and retrieved from the CERN Accelerator Logging Service. The origin point of the primary source corresponded to the location of the SEC used to monitor the beam intensity which is located approximately 23 m upstream the target: between the source point and the target, the beam is travelling through air.

Neutron fluence energy spectra at the activation detector installation locations were estimated using track-length estimators of 10 cm diameter spheres: the spectra were estimated from 0.01 meV in FLUKA, and from 0.1 MeV in PHITS and GEANT4. The ^{24}Na production yield was then estimated by weighting the obtained neutron fluence energy spectra with the evaluated cross section of the ^{27}Al$(n,\alpha)^{24}$Na reaction from the Meakawa library [24] shown in Fig. 7, which is based on experimental data by Kim et al. [25].

4. Results and discussion

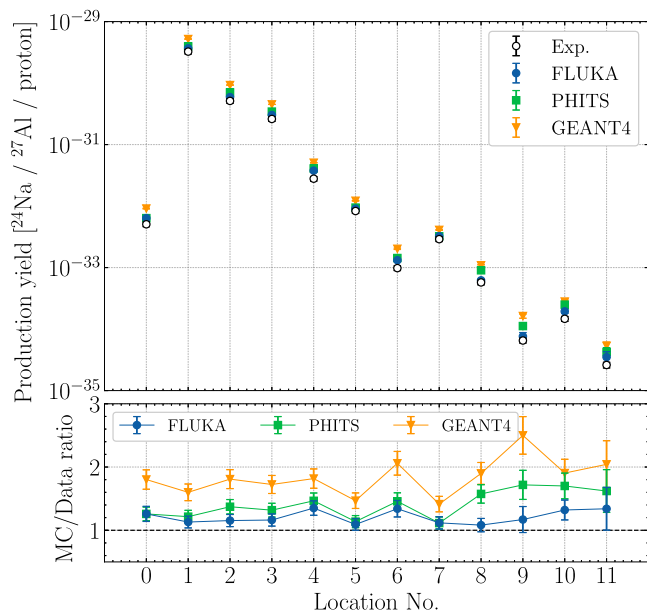The numerical values of the measured ^{24}Na production yields per ^{27}Al atom and per primary proton [^{24}Na/^{27}Al/proton] are summarized in Table 2 and the corresponding attenuation profile along the maze legs can be observed in Fig. 8. The reported uncertainties on the experimental values are related to the gamma spectroscopy counting (from 0.4% to 6.5%), to the HPGe-detector efficiency calibration (of the order of 4.3%), and to the secondary emission chamber calibration (of the order of 7.0%). Uncertainties on the beam momentum, beam position and spatial profile, and target dimensions are well below 1%.

For comparison, the production yields calculated with FLUKA, PHITS, and GEANT4 are also summarized in Table 2 and illustrated in Fig. 8 alongside the experimental results: the uncertainties of the results of the Monte Carlo simulations are of statistical nature. In general, the three Monte Carlo codes follow qualitatively the same trend of the experimental data but some discrepancies can be observed. To better discuss the differences, the ratios between the values calculated with the Monte Carlo codes and the experimental data (MC/Data ratios) are also presented in Fig. 8 and summarized for convenience in Table 3.

It can be observed that the calculated results with FLUKA and PHITS are generally in very good agreement with each other. They both also reasonably agree with the experimental results over the maze legs, with FLUKA being closest to the experimental results and always within a factor 1.4. In particular, the MC/Data ratios for the two codes remain below 1.5 up to location 7, while they tend to become larger for more shielded locations: even in the worst case, the MC/Data ratio for PHITS remains below 1.72. For GEANT4, instead, larger differences are observed, with the MC/Data ratios ranging from 1.41 to 2.5. Since, however, the comparison with experimental data for the three codes essentially follows the same trend, this difference may be attributed mainly to the neutron production by the primary protons in the target, which could be caused by differences in nuclear models, parameters, and databases for secondary particle production. A similar behaviour between the three Monte Carlo codes had also been observed in shielding penetration studies [4].

Finally, it is important to comment on the trend of the attenuation profile observed in the maze. Fig. 9 illustrates the spatial distribution at beam height of the ^{24}Na production yield as simulated with FLUKA: since the production cross section exhibits a threshold of approximately 4 MeV as displayed in Fig. 7, this spatial distribution allows to have a better overview of the high-energy neutron fluence. High production

Table 2
Numerical values of the ^{24}Na production yield per ^{27}Al atom and per primary proton as experimentally measured and as calculated via FLUKA, PHITS, and GEANT4.

No.	Experiment		FLUKA		PHITS		GEANT4	
	[^{24}Na/^{27}Al/proton]	[%]	[^{24}Na/^{27}Al/proton]	[%]	[^{24}Na/^{27}Al/proton]	[%]	[^{24}Na/^{27}Al/proton]	[%]
0	5.06×10^{-33}	8.43	6.37×10^{-33}	4.31	6.37×10^{-33}	1.43	9.12×10^{-33}	1.22
1	3.25×10^{-30}	8.22	3.67×10^{-30}	0.18	3.95×10^{-30}	0.06	5.20×10^{-30}	0.05
2	5.13×10^{-31}	8.28	5.92×10^{-31}	0.44	7.04×10^{-31}	0.14	9.28×10^{-31}	0.12
3	2.61×10^{-31}	8.26	3.03×10^{-31}	0.62	3.44×10^{-31}	0.21	4.50×10^{-31}	0.17
4	2.79×10^{-32}	8.41	3.77×10^{-32}	0.87	4.09×10^{-32}	0.50	5.07×10^{-32}	0.44
5	8.31×10^{-33}	8.33	9.07×10^{-33}	1.36	9.45×10^{-33}	1.05	1.22×10^{-32}	0.89
6	9.81×10^{-34}	8.75	1.32×10^{-33}	4.22	1.43×10^{-33}	3.04	2.02×10^{-33}	2.50
7	2.90×10^{-33}	8.53	3.24×10^{-33}	1.69	3.23×10^{-33}	1.70	4.10×10^{-33}	1.44
8	5.74×10^{-34}	8.53	6.21×10^{-34}	4.68	9.04×10^{-34}	3.60	1.09×10^{-33}	3.16
9	6.52×10^{-35}	8.89	7.63×10^{-35}	15.15	1.12×10^{-34}	10.00	1.63×10^{-34}	7.88
10	1.47×10^{-34}	9.27	1.94×10^{-34}	7.46	2.50×10^{-34}	7.52	2.80×10^{-34}	6.68
11	2.61×10^{-35}	10.48	3.50×10^{-35}	22.93	4.23×10^{-35}	18.06	5.33×10^{-35}	15.02

Table 3
Numerical values of the ratios between the ^{24}Na production yields calculated with the Monte Carlo codes and the experimental data (MC/Data ratios). The reported uncertainties are absolute uncertainties.

No.	FLUKA/Exp.	PHITS/Exp.	GEANT4/Exp.
0	1.26 ± 0.12	1.26 ± 0.11	1.80 ± 0.15
1	1.13 ± 0.09	1.22 ± 0.10	1.60 ± 0.13
2	1.15 ± 0.10	1.37 ± 0.11	1.81 ± 0.15
3	1.16 ± 0.10	1.32 ± 0.11	1.72 ± 0.14
4	1.35 ± 0.11	1.47 ± 0.12	1.82 ± 0.15
5	1.09 ± 0.09	1.14 ± 0.10	1.47 ± 0.12
6	1.34 ± 0.13	1.46 ± 0.13	2.06 ± 0.19
7	1.12 ± 0.10	1.11 ± 0.10	1.41 ± 0.12
8	1.08 ± 0.11	1.57 ± 0.15	1.90 ± 0.17
9	1.17 ± 0.21	1.72 ± 0.23	2.50 ± 0.30
10	1.32 ± 0.16	1.70 ± 0.20	1.90 ± 0.22
11	1.34 ± 0.34	1.62 ± 0.34	2.04 ± 0.37

rates at location from 1 to 3 are clearly due to the fact the activation detectors were in direct view of the target. The production yield at location 0 is almost two orders of magnitude lower than the one at location 3 since the angle with respect to the beam impact point is larger than 90° and the contribution from penetrating neutrons is smaller since they have to traverse concrete and iron shielding layers. Looking at the isolines in Fig. 9, it is also possible to notice that for locations 4, 5, 7, 8, and 10 the contribution from the high-energy neutron penetration through the shielding is still significant. Instead, the production yield at location 6 is lower than at the two neighbouring ones because the shielding thickness in the line of sight of the target is greater and thus the contribution from high-energy penetrating neutrons is suppressed. To support these considerations, Fig. 10 shows the neutron fluence energy spectra above 1 MeV as simulated with FLUKA: since the spectra span several orders of magnitude, only the ones for locations from 0 to 7 are illustrated for better visualization purposes.

5. Conclusions

The design of shielding structures of particle accelerators is an aspect of the utmost importance to ensure their safe and reliable operation. As Monte Carlo radiation transport codes are now the state-of-the-art tools for radiation protection assessments, particularly at high-energy facilities, the validation of the calculation results is an equally important aspect to better establish safety margins of design studies.

This work has described the results of the high-energy neutron streaming experiments conducted in 2022 at the CHARM facility at CERN, where secondary neutrons are produced by the impact of a high-intensity 24 GeV/c proton beam on a 50 cm long copper target. Measuring the production yield of ^{24}Na in high-purity aluminium activation detectors allowed to reconstruct the neutron attenuation profile

in the various legs of the access maze up to very distant areas from the beam impact point. Monte Carlo simulations were performed with FLUKA, PHITS and GEANT4: comparisons between experimental and simulated results revealed consistent trends across different codes and reasonable agreement with the measurements within a factor 1.4, 1.72 and 2.5 respectively. Additionally, the simulations allowed to assess that the contribution from neutrons penetrating the lateral parts of the shield can still be important even at distant locations.

In conclusion, the results presented in this work increase the availability of neutron streaming benchmark data for high-energy facilities, and, thanks to the extensive code intercomparison performed, provide valuable input for the design studies of future accelerator facilities.

CRediT authorship contribution statement

D. Bozzato: Writing – review & editing, Writing – original draft, Supervision, Software, Investigation, Data curation, Conceptualization. **A. Devienne:** Supervision, Project administration, Investigation. **R. Froeschl:** Supervision, Resources, Project administration, Investigation, Conceptualization. **A. Infantino:** Supervision, Investigation, Conceptualization. **T. Lorenzon:** Supervision, Investigation. **F. Pozzi:** Supervision, Investigation. **M. Tisi:** Supervision, Investigation. **N. Nakao:** Supervision, Software, Methodology, Investigation, Formal analysis, Data curation, Conceptualization. **T. Kajimoto:** Software, Investigation, Data curation, Conceptualization. **T. Sanami:** Supervision, Investigation, Conceptualization. **S. Roesler:** Supervision, Project administration. **M. Brugger:** Supervision, Project administration.

Declaration of competing interest

The authors declare that they have no known competing financial interests or personal relationships that could have appeared to influence the work reported in this paper.

Data availability
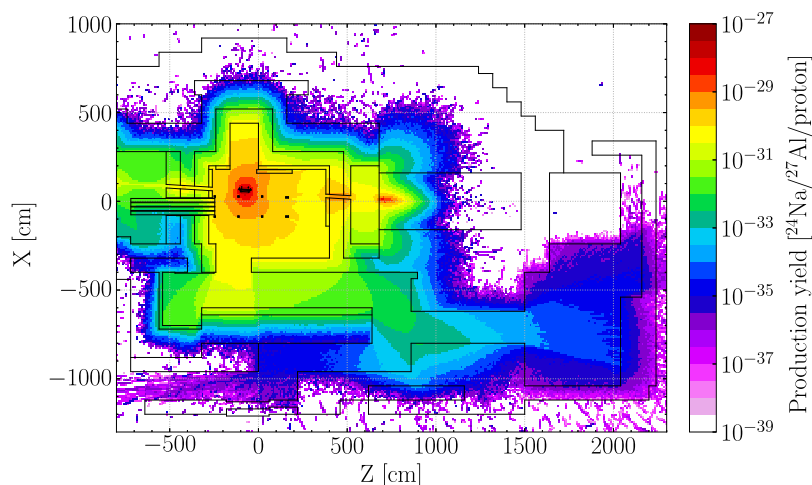
Data will be made available on request.

Fig. 9. Spatial distribution at beam height of the ^{24}Na production yield per ^{27}Al atom and per primary proton as simulated with FLUKA.
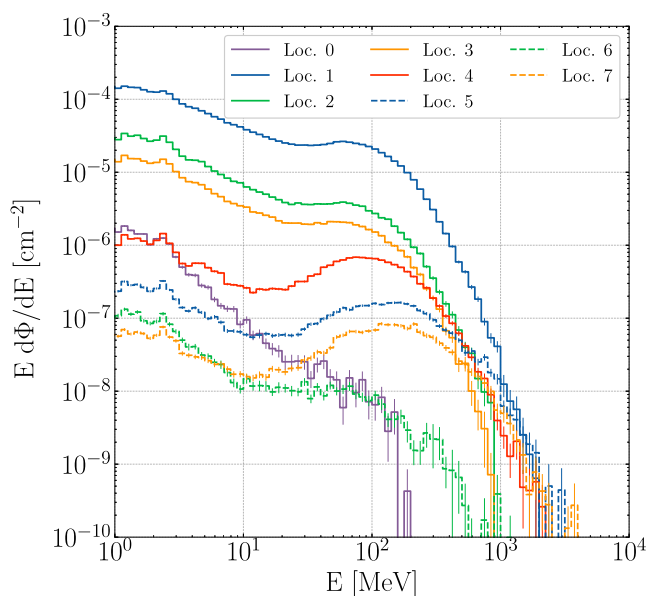

Fig. 10. Neutron fluence energy spectra above 1 MeV as simulated with FLUKA for locations from 0 to 7.

References

[1] A.H. Sullivan, Guide to radiation and radioactivity levels near high energy particle accelerators, Nucl. Techn. Publ., Ashford, 1992.

[2] R. Froeschl, M. Brugger, S. Roesler, The CERN high energy accelerator mixed field (CHARM) facility in the CERN PS East Experimental Area, in: Proceedings of the 12th Meeting of the Task-Force on Shielding Aspects of Accelerators, Targets and Irradiation Facilities (SATIF12), NEA/NSC/R(2015)3, 2015, pp. 14–25.

[3] T. Matsumoto, A. Masuda, E. Lee, T. Sanami, et al., Measurement of neutron spectra for various thicknesses of concrete and steel shielding at 24-GeV/c proton beam facility using Bonner sphere spectrometer, J. Nucl. Sci. Technol. 61 (1) (2024) 98–110, http://dx.doi.org/10.1080/00223131.2023.2274933.

[4] N. Nakao, T. Sanami, T. Kajimoto, H. Yashima, R. Froeschl, D. Bozzato, E. Iliopoulou, A. Infantino, E. Lee, T. Oyama, M. Hagiwara, S. Nagaguro, T. Matsumoto, A. Masuda, Y. Uwamimno, S. Roesler, M. Brugger, Measurement and simulations of high-energy neutrons through a various thickness of concrete and steel shield using activation detectors at CHARM, J. Nucl. Sci. Technol. 61 (4) (2024) 429–447, http://dx.doi.org/10.1080/00223131.2023.2239243.

[5] N. Nakao, T. Kajimoto, T. Sanami, R. Froeschl, E. Iliopoulou, et al., Measurements and Monte Carlo simulations of high-energy neutron streaming through the access maze using activation detectors at 24 GeV/c proton beam facility of CERN/CHARM, J. Nucl. Sci. Technol. 58 (8) (2021) 899–907, http://dx.doi.org/10.1080/00223131.2021.1887003.

[6] B. Gkotse, M. Glaser, P. Lima, E. Matli, M. Moll, F. Ravotti, A new high-intensity proton irradiation facility at the CERN PS east area, PoS TIPP2014 (AIDA-CONF-2014-019) (2014) 354, http://dx.doi.org/10.22323/1.213.0354.

[7] A. Curioni, R. Froeschl, M. Glaser, E. Iliopoulou, F. La Torre, F. Pozzi, F. Ravotti, M. Silari, Single- and multi-foils ^{27}Al(p,3pn)^{24}Na activation technique for monitoring the intensity of high-energy beams, Nucl. Instrum. Methods Phys. Res. A 858 (2017) 101–105, http://dx.doi.org/10.1016/j.nima.2017.03.058.

[8] F. Ravotti, R. Brice Ruffieux, A. Ollacarizqueta Guerrero, Calibration of the T08.XSEC devices by means of Al-foil activation and BCTF measurements, Tech. Rep EP-Tech-Note-2022-001, CERN, Geneva, 2022.

[9] F. Bronson, Validation of the accuracy of the labsocs software for mathematical efficiency calibration of ge detectors for typical laboratory samples, J. Radioanal. Nucl. Chem. 255 (2003) 137–141, http://dx.doi.org/10.1023/A:1022248318741.

[10] C. Ahdida, D. Bozzato, D. Calzolari, F. Cerutti, N. Charitonidis, A. Cimmino, A. Coronetti, G. D'Alessandro, A. Donadon Servelle, L. Esposito, R. Froeschl, et al., New capabilities of the FLUKA multi-purpose code, Front Phys 9 (2022) 788253, http://dx.doi.org/10.3389/fphy.2021.788253.

[11] G. Battistoni, T. Boehlen, F. Cerutti, P.W. Chin, L. Esposito, A. Fassò, A. Ferrari, A. Lechner, A. Empl, et al., Overview of the FLUKA code, Ann. Nucl. Energy 82 (2015) 10–18, http://dx.doi.org/10.1016/j.anucene.2014.11.007.

[12] T. Sato, Y. Iwamoto, S. Hashimoto, T. Ogawa, T. Furuta, S. Abe, T. Kai, P.-E. Tsai, N. Matsuda, H. Iwase, et al., Features of particle and heavy ion transport code system (PHITS) version 3.02, J. Nucl. Sci. Technol. 55 (6) (2018) 684–690, http://dx.doi.org/10.1080/00223131.2017.1419890.

[13] Y. Iwamoto, T. Sato, S. Hashimoto, T. Ogawa, T. Furuta, S. Abe, T. Kai, P.-E. Tsai, N. Matsuda, R. Hosoyamada, K. Niita, Benchmark study of the recent version of the PHITS code, J. Nucl. Sci. Technol. 54 (5) (2017) 617–635, http://dx.doi.org/10.1080/00223131.2017.1297742.

[14] J. Allison, et al., Recent developments in Geant4, Nucl. Instrum. Methods Phys. Res. A: Accel. Spectrom. Detect. Assoc. Equip. 835 (2016) 186–225, http://dx.doi.org/10.1016/j.nima.2016.06.125.

[15] J. Allison, et al., Geant4 developments and applications, IEEE Trans. Nucl. Sci. 53 (2006) 270–278, http://dx.doi.org/10.1109/TNS.2006.869826.

[16] V. Vlachoudis, the FLUKA CERN Collaboration, Recent developments in the point wise neutron treatment for FLUKA v4, EPJ Web Conf. 284 (2023) 03021, http://dx.doi.org/10.1051/epjconf/202328403021.

[17] E. Mendoza, D. Cano-Ott, T. Koi, C. Guerrero, New standard evaluated neutron cross section libraries for the GEANT4 code and first verification, IEEE Trans. Nucl. Sci. 61 (4) (2014) 2357–2364, http://dx.doi.org/10.1109/TNS.2014.2335538.

[18] E. Mendoza, D. Cano-Ott, C. Guerrero, R. Capote, New Evaluated Neutron Cross Section Libraries for the Geant4 Code, Tech. rep, IAEA, 2012, Technical report - INDC(NDS)-0612.

[19] E. Mendoza, D. Cano-Ott, Update of the Evaluated Neutron Cross Section Libraries for the Geant4 Code, Technical report INDC(NDS)-0758, IAEA, 2018.

[20] S. Furihata, Statistical analysis of light fragment production from medium energy proton-induced reactions, Nucl. Instrum. Methods Phys. Res. B 171 (3) (2000) 251–258, http://dx.doi.org/10.1016/S0168-583X(00)00332-3.

[21] A. Boudard, J. Cugnon, J.-C. David, S. Leray, D. Mancusi, New potentialities of the Liège intranuclear cascade model for reactions induced by nucleons and light charged particles, Phys. Rev. C 87 (2013) 014606, http://dx.doi.org/10.1103/PhysRevC.87.014606.

[22] Y. Nara, N. Otuka, A. Ohnishi, K. Niita, S. Chiba, Relativistic nuclear collisions at $10A$ GeV energies from p+Be to Au+Au with the hadronic cascade model, Phys. Rev. C 61 (1999) 024901, http://dx.doi.org/10.1103/PhysRevC.61.024901.

[23] K. Shibata, O. Iwamoto, T. Nakagawa, N. Iwamoto, A. Ichihara, S. Kunieda, S. Chiba, K. Furutaka, N. Otuka, T. Ohsawa, T. Murata, H. Matsunobu, A. Zukeran, S. Kamada, J.-I. Katakura, JENDL-4.0: A new library for nuclear science and engineering, J. Nucl. Sci. Technol. 48 (1) (2011) 1–30, http://dx.doi.org/10.1080/18811248.2011.9711675.

[24] F. Maekawa, U. von Mollendorff, P. Wilson, M. Wada, Y. Ikeda, Production of a dosimetry cross section set up to 50 MeV, Proc. 10th International Symposium on Reactor Dosimetry, Sep 12-17, 1999, Osaka, Japan, 2001.

[25] E. Kim, T. Nakamura, Y. Uwamino, et al., Neutron activation cross section of ^{12}C,^{27}Al,^{59}Co,^{nat}Cu and^{209}Bi nuclides in the energy range 20 MeV to 200 MeV, Proc. Int. Conf. Nucl. Data Sci. Technol. (1997) 1503–1507.